

# We are IntechOpen, the world's leading publisher of Open Access books Built by scientists, for scientists

5,800

Open access books available

142,000

International authors and editors

180M

Downloads

Our authors are among the

154

Countries delivered to

TOP 1%

most cited scientists

12.2%

Contributors from top 500 universities



WEB OF SCIENCE™

Selection of our books indexed in the Book Citation Index  
in Web of Science™ Core Collection (BKCI)

Interested in publishing with us?  
Contact [book.department@intechopen.com](mailto:book.department@intechopen.com)

Numbers displayed above are based on latest data collected.  
For more information visit [www.intechopen.com](http://www.intechopen.com)



# Active Vibration Suppression Based on Piezoelectric Actuator

*Min Wang, Songquan Liao, Xuan Fang and Shibo Fu*

## Abstract

The piezoelectric constitutive equation states that the inverse piezoelectric effect can convert electrical energy into mechanical energy, resulting in small displacement and force changes with high resolution. The piezoelectric actuator based on inverse piezoelectric effect has an excellent performance in active vibration suppression because of its high frequency response, high positioning accuracy, and large output force. A new active-passive composite vibration suppression system can be formed by cascading it with passive vibration isolation elements in series and parallel. On this basis, by adding different control algorithms and control loops, such as the Sky-Hook damping feedback control algorithm and adaptive feedforward control algorithm, different vibration control effects can be realized.

**Keywords:** vibration isolation, active control, active-passive, inverse piezoelectric effect, piezoelectric actuator

## 1. Introduction

Mechanical vibration exists in various machines in working conditions, such as precision machine tools, aircrafts, ships, etc. Strong vibration will affect the accuracy and stability of mechanical parts. In severe cases, it will also lead to fatigue failure and shorten the life of the structure or cause resonance to damage the structure. Therefore, suppressing the unfavorable vibration response has become an urgent problem to be solved in the industry.

The passive vibration suppression system commonly used in the engineering field achieves the purpose of vibration suppression by installing elastic damping elements to consume and absorb vibration energy. The system has high reliability but cannot adjust the vibration suppression characteristics and cannot adapt to changes in the external environment. Therefore, the active vibration suppression system with active adjustment capability and wide adaptive frequency range has become a research hotspot.

The active vibration suppression system is composed of sensors, actuators, and control systems, so the current research mainly focuses on two directions. One is the study of active control strategies; the other is the study of new materials and corresponding actuators. The active control strategies currently used in the field of

vibration suppression include PID control [1], adaptive control [2, 3], intelligent control [4, 5], and so on. The actuator is one of the key elements that affect the vibration suppression performance of the entire active vibration suppression system. In recent years, the development of smart material structures has provided conditions for the development of actuators, which has greatly promoted the research and application of active vibration control technology. At present, the smart materials used in the design of active vibration suppression actuators mainly include electro/magneto-rheological fluids [6, 7], shape memory alloys [8, 9], magnetostrictive materials [10, 11], piezoelectric materials [12], and so on. Among them, the piezoelectric materials can be used as both actuators (inverse piezoelectric effect) and sensors (positive piezoelectric effect) due to their positive and inverse piezoelectric effects. As actuators, they have many advantages such as fast frequency response, wide control frequency range, high displacement resolution, small size, easy integration, no mechanical friction, and so on [13]. They have been widely used in active vibration suppression systems.

Most of the active suppression methods based on piezoelectric actuators reduce the vibration by directly suppressing the excitation force. That is, when the piezoelectric actuators are arranged, the direction of the output force/displacement of the actuators is consistent with the direction of the system vibration. In order to improve the vibration suppression effect, it is usually required that the piezoelectric actuator can output a sufficiently large displacement and control force at the same time, but its realization is limited by the electromechanical coupling characteristics of the piezoelectric actuator. This chapter discusses an active-passive composite vibration suppression system based on piezoelectric actuators. The active control element adopts a piezoelectric stack actuator with a mechanical displacement amplifying mechanism. The piezoelectric stack actuator has the advantages of high energy conversion efficiency, low operating voltage, and large output force. The mechanical displacement amplifying mechanism has a compact structure and can effectively amplify the displacement of the actuator. The second section of the chapter will analyze the driving characteristics of the piezoelectric actuator and the magnification of the displacement amplifying mechanism in the active control element, and discuss the compensation of hysteresis that affects the control accuracy of the piezoelectric actuator. Section 3 will analyze and construct the structure of the active-passive composite vibration suppression system based on the piezoelectric actuator, and establish its dynamic model. Section 4 will analyze the vibration control theory of the active-passive composite vibration suppression system using different control algorithms and control loops on the basis of the system dynamics model, and simulate the effectiveness of the algorithms. Section 5 will build an experimental platform to verify the active vibration suppression effect of the active-passive composite vibration suppression system based on the piezoelectric actuator. Section 6 is the conclusion, which will summarize the content of this chapter.

## **2. Characteristics of piezoelectric actuator in vibration suppression**

### **2.1 Inverse piezoelectric effect of piezoelectric actuator**

The piezoelectric constitutive equation states that the inverse piezoelectric effect of piezoelectric actuators can convert electrical energy into mechanical energy, resulting in small displacement and force changes with high resolution.

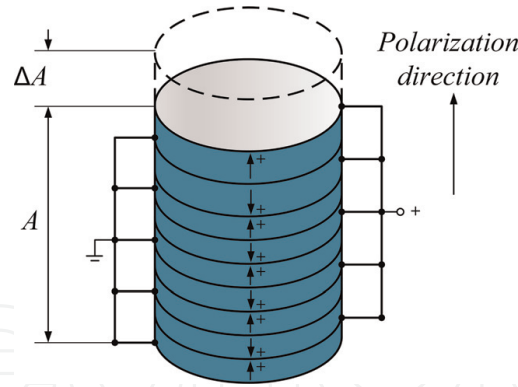


**Figure 1.**  
 Structure diagram of piezoelectric stack actuator.

The piezoelectric stack actuator used in this chapters is formed by stacking many thin piezoelectric ceramic sheets, and its structure is shown in **Figure 1**. Each piezoelectric ceramic sheet is equipped with electrodes and is separated by an insulating layer. The elongation of the piezoelectric ceramic sheet along the polarization direction is mainly related to the applied electric field strength but has nothing to do with its thickness. With the layered stack structure, the elongation of the piezoelectric ceramic sheets can be accumulated, so that the piezoelectric stack actuator can still generate a relatively large displacement at a lower operating voltage.

According to the inverse piezoelectric effect of piezoelectric materials, only considering the longitudinal force and elongation of the piezoelectric ceramic sheet under the action of the driving voltage, and assuming that the strain is uniformly distributed in the longitudinal polarization direction, then the longitudinal stress of a single piezoelectric ceramic sheet can be expressed as:

$$\sigma = E_p(\varepsilon - d_{33}E) \quad (1)$$

where  $\sigma$  is the longitudinal stress;  $E_p$  is the initial elastic modulus;  $\varepsilon$  is the longitudinal strain;  $d_{33}$  is the longitudinal piezoelectric strain constant;  $E$  is the longitudinal electric field strength.

Assuming that the force-bearing area of the piezoelectric ceramic sheet is  $A_p$ , the thickness is  $h$ , the voltage applied at both ends is  $V$  and the resulting thickness deformation is  $\delta$ . Then the longitudinal strain  $\varepsilon$  and longitudinal electric field strength  $E$  in Eq. (1) can be expressed as:

$$\varepsilon = \delta/h \quad (2)$$

$$E = V/h \quad (3)$$

The force on the piezoelectric ceramic sheet can be expressed as the stress  $\sigma$  multiplied by the force-bearing area  $A_p$ , and the relationship between the output force and the force on the piezoelectric ceramic sheet is force and reaction force. Combining Eqs. (1–3), the output force of the piezoelectric ceramic sheet is:

$$f = -\sigma A_p = A_p E_p / h (d_{33} V - \delta) \quad (4)$$

Let  $k = A_p E_p / h$ , which is the inherent constant of the piezoelectric ceramic sheet, the output force expression of the piezoelectric ceramic sheet can be simplified as:

$$f = k(d_{33}V - \delta) \quad (5)$$

According to the output force expression Eq. (5), the output displacement of the piezoelectric ceramic sheet can be obtained as:

$$\delta = d_{33}V - f/k \quad (6)$$

Since the piezoelectric stack actuator cascades several piezoelectric ceramic sheets in voltage parallel and physical series, its output force is the same as that of a single piezoelectric ceramic sheet, and its output displacement is the sum of the output displacement of all piezoelectric ceramic sheets:

$$\begin{cases} f_z = f \\ \Delta A = n\delta \end{cases} \quad (7)$$

where  $f_z$  is the output force of the piezoelectric actuator,  $\Delta A$  is the output displacement of the piezoelectric actuator, and  $n$  is the number of piezoelectric ceramic sheets in the piezoelectric actuator.

Although the output displacement of the piezoelectric stack actuator is the sum of the output displacements of all piezoelectric ceramic sheets, its stroke is still in the order of microns. In practical applications, it is usually necessary to cooperate with a displacement amplifying mechanism [14–16]. Therefore, it is necessary to analyze the displacement amplification characteristics of the displacement amplifying mechanism.

## 2.2 Displacement amplifying mechanism of piezoelectric actuator

The mechanical displacement amplifying mechanism adopted in this chapter is based on the principle of triangular amplification to mechanically amplify the displacement of the piezoelectric actuator, to make up for the shortcoming of its insufficient stroke and expand its effective stroke. Dimensions such as the coordinate direction and angle of the displacement amplifying mechanism are shown in **Figure 2a**. The piezoelectric stack actuator with length  $A$  is placed in the  $x$ -direction of the displacement amplifying mechanism, and the inclination angle formed by the horizontal direction and the hypotenuse of the amplifying mechanism is  $\alpha$ .

The amplification principle of the mechanical displacement amplifying mechanism is shown in **Figure 2b**. When the displacement changes in the  $x$ -direction, the inverse change of the displacement occurs in the  $y$ -direction. The displacement magnification

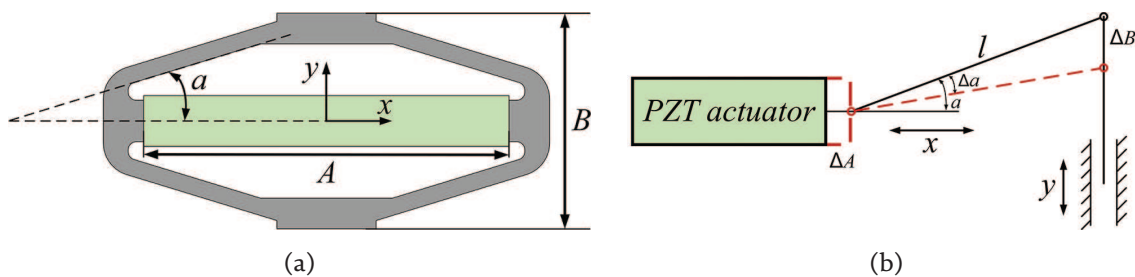


**Figure 2.** Displacement amplifying mechanism: (a) dimension labeling diagram; (b) amplifying schematic diagram.

is defined as the ratio of the displacement change in the  $y$ -direction to the displacement change in the  $x$ -direction, which can be expressed as:

$$\gamma = \frac{\Delta B}{\Delta A} \quad (8)$$

According to the geometric transformation relationship shown in **Figure 2b**, we can get:

$$\begin{aligned} \Delta A &= l \cos \alpha - l \cos (\alpha - \Delta \alpha) \\ \Delta B &= l \sin \alpha - l \sin (\alpha - \Delta \alpha) \end{aligned} \quad (9)$$

Then the displacement magnification can be organized as:

$$\gamma = \frac{\Delta B}{\Delta A} = \frac{l \sin \alpha - l \sin (\alpha - \Delta \alpha)}{l \cos \alpha - l \cos (\alpha - \Delta \alpha)} = \frac{\tan \alpha (1 - \cos (\Delta \alpha)) + \sin (\Delta \alpha)}{1 - \cos (\Delta \alpha) - \tan \alpha \sin (\Delta \alpha)} \quad (10)$$

Since the stroke of the piezoelectric actuator is in the order of microns, the variation in length  $\Delta A$  and the variation in inclination angle  $\Delta \alpha$  are quite small. According to the equivalent infinitesimal principle:  $\sin (\Delta \alpha) \approx \Delta \alpha$ ,  $1 - \cos (\Delta \alpha) \approx \frac{1}{2} (\Delta \alpha)^2$ ,  $\tan (\Delta \alpha) \approx \Delta \alpha$ . The Eq. (10) can be further organized as:

$$\gamma = \frac{\Delta \alpha \tan \alpha + 2}{\Delta \alpha - 2 \tan \alpha} \approx -\frac{1}{\tan \alpha} \quad (11)$$

It can be seen from Eq. (11) that the magnification of the triangular mechanical displacement amplifying mechanism is not related to the length but is only related to the size of the inclination angle  $\alpha$ . The negative sign indicates that the displacement changes in the  $y$ - and  $x$ -directions are opposite. The relationship between magnification and inclination angle is described in **Figure 3**.

It can be seen from **Figure 3** that the smaller the inclination angle, the larger the magnification (regardless of positive and negative). As the inclination angle increases, the change in magnification becomes insignificant. When the inclination angle reaches 45 degrees, the magnification is close to 1.

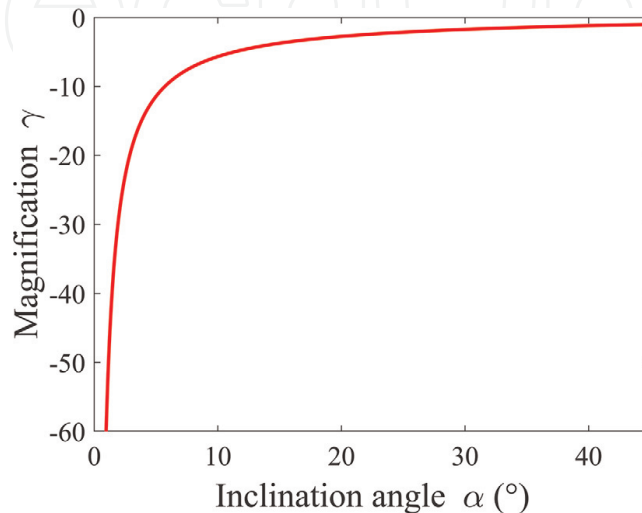


**Figure 3.**  
 Relationship between magnification and inclination angle.



### 2.3 Compensation of hysteresis in piezoelectric actuator

According to Eqs. (6–7), under ideal conditions, the output displacement of the piezoelectric actuator is proportional to the driving voltage, as shown by the red solid line in **Figure 4**. But, in fact, due to the difference in structure and the complexity of its working mechanism, piezoelectric actuators have the inherent characteristics of hysteresis [17], which leads to the fact that the voltage rise and drop curve of the output displacement do not overlap, as shown by the green and blue lines in **Figure 4**. This affects the control accuracy of the piezoelectric actuator to a certain extent. In general engineering applications, the displacement error is relatively small, and the piezoelectric actuator can be used approximately linearly. However, in some applications that require high control accuracy, it is necessary to perform hysteresis compensation [18–21]. The hysteresis in the piezoelectric actuator can be compensated by the hysteresis inverse compensation method. The specific compensation control block diagram is shown in **Figure 5**. This method can avoid complex modeling and parameter identification of the piezoelectric actuator, and the error output can be directly used for compensation control to achieve the effect of eliminating hysteresis and improve the control accuracy of the piezoelectric actuator.

### 3. Active-passive composite vibration suppression system based on piezoelectric actuator

The passive vibration suppression system has a simple structure and good high-frequency vibration suppression performance, but it is powerless to low-frequency vibration, and the resonance peak suppression conflicts with high-frequency vibration suppression. The vibration suppression performance of the active vibration suppression system is good, but due to the limitation of the working bandwidth and power of the actuator, it is difficult to realize the active vibration suppression only. Therefore, active actuators are usually used in combination with passive elements to form an active-passive composite vibration suppression system to achieve the best vibration suppression effect [22–24].

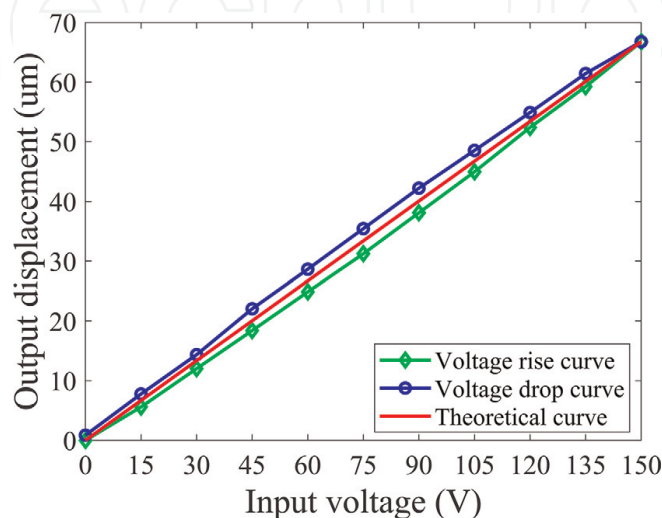


**Figure 4.**  
*The relationship between voltage and displacement of piezoelectric actuator.*

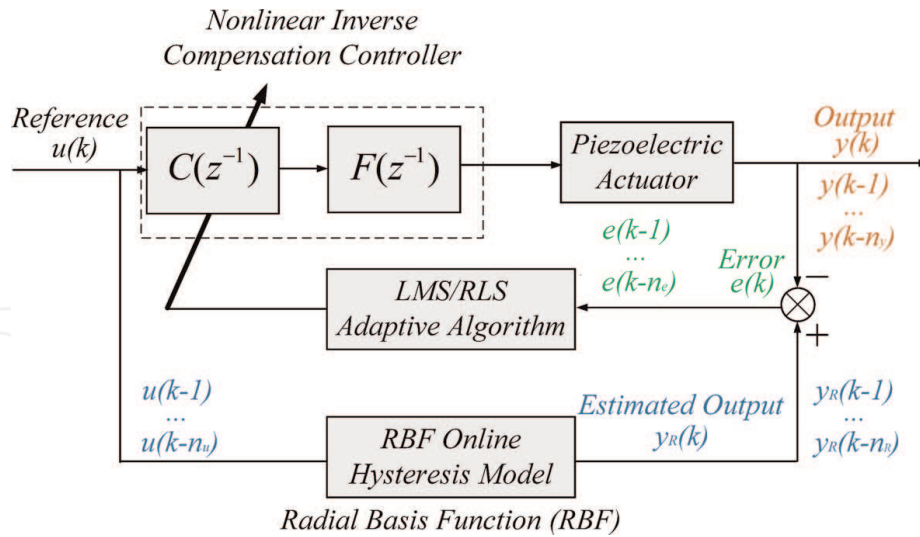


**Figure 5.** Hysteresis adaptive inverse compensation control block diagram of piezoelectric actuator.

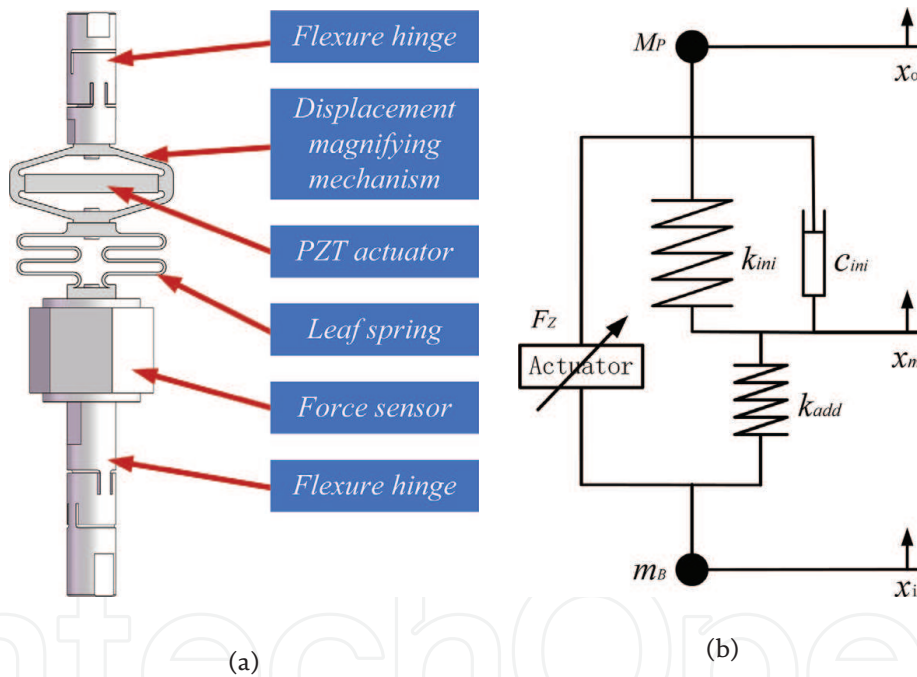


**Figure 6.** Single-degree-of-freedom vibration suppression system: (a) three-dimensional model diagram; (b) simplified model diagram.

The active control element based on the piezoelectric actuator has high stiffness. In order to reduce the overall stiffness of the vibration suppression system, thereby reducing the natural frequency of the system and increasing the vibration suppression bandwidth, the active control element and the leaf spring with relatively low stiffness are connected in series to form a vibration suppression system with an active-passive composite structure in this paper, as shown in **Figure 6a**. The vibration suppression system is a single-degree-of-freedom system. The modular design reduces the mass and size of the system to the greatest extent, which makes it more suitable for applications in those fields with strict space and mass constraints, such as aerospace, ships, etc. In addition, according to the needs of the application, it can be conveniently used as the branch chain of the multi-degree-of-freedom vibration suppression



platform through the flexible hinges [13, 25–27]. Its simplified model is shown in **Figure 6b**.

According to Newton's second law, the dynamic equation of the system can be obtained as:

$$\begin{cases} M_p \ddot{x}_o + c_{ini}(\dot{x}_o - \dot{x}_m) + k_{ini}(x_o - x_m) = F_z \\ c_{ini}(\dot{x}_o - \dot{x}_m) + k_{ini}(x_o - x_m) = k_{add}(x_m - x_i) \end{cases} \quad (12)$$

where  $M_p$  is the load mass,  $c_{ini}$  is the initial damping of the system,  $k_{ini}$  is the initial stiffness of the system,  $k_{add}$  is the additional stiffness of the leaf spring,  $x_o$  is the load displacement,  $x_m$  is the displacement of the connection point between the displacement amplifying mechanism and the leaf spring,  $x_i$  is the base displacement,  $F_z$  is the output force of the active control element.

By combining the two equations in Eq. (12) and eliminating the relevant variables at the intermediate connection point, the dynamic model of the single-degree-of-freedom vibration suppression system is obtained as follows:

$$M_p \ddot{x}_o + c(\dot{x}_o - \dot{x}_i) + k_d(x_o - x_i) = F_z \quad (13)$$

where  $c = k_{add}c_{ini}/(k_{add} + k_{ini})$  is the equivalent damping of the system and  $k_d = k_{add}k_{ini}/(k_{add} + k_{ini})$  is the equivalent stiffness of the system.

It can be seen from Eq. (13) that the active control element in series with the leaf spring can effectively reduce the overall stiffness of the vibration suppression system, and the establishment of the structure and dynamic model of the active-passive composite vibration suppression system provides the object and theoretical basis for the subsequent active vibration suppression control.

## 4. Active vibration suppression control based on piezoelectric actuator

### 4.1 Piezoelectric active vibration suppression system

Passive vibration suppression refers to the introduction of one or more mass-spring damping systems in the propagation path of the vibration source. Although this technical solution is simple and reliable, it can only effectively attenuate high-frequency vibrations in a wide frequency band. With the rapid development of smart sensors and smart actuators and high-speed microprocessors, active vibration suppression is becoming more and more attractive in vibration suppression. In piezoelectric active control, it is classified according to the control structure, which can be divided into feedforward control and feedback control. In precision vibration isolation, different vibration active control structures need to be adopted for different vibration isolation objects in actual work.

In the piezoelectric active vibration suppression system, the overall control block diagram of feedforward and feedback is shown in **Figure 7**. In **Figure 7**, The vibration suppression closed-loop consists of a table feedback loop with a signal filter function and a ground-based feedforward loop with a signal filter function. The feedback loop is implemented as: The feedback acquisition sensor collects the table vibration, and then filters the excess noise signal, and then transmits it to the feedback controller for algorithm calculation, and adjusts the gain of the entire feedback loop to change the feedback characteristics. The implementation of the feedforward loop is as follows:

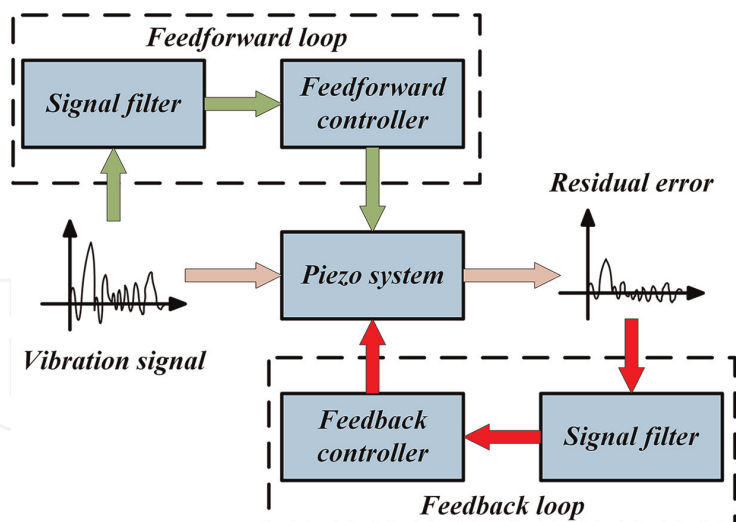


**Figure 7.**  
 Piezoelectric active vibration suppression control block diagram.

The feedforward acquisition sensor collects the ground vibration signal, then filters the excess noise signal, and then transmits it to the feed-forward controller for algorithm calculation, and adjusts the feedforward control parameters to change the feedforward characteristics. The piezoelectric feedback active control algorithm can be realized by sky-hook damping, integral force feedback (IFF), and other algorithms, and the feedforward control algorithm can be realized by adaptive control algorithm or phase compensation algorithm. Finally, the hybrid operation of the two active controllers is output to the piezoelectric actuator, and the active vibration suppression system is controlled to complete the active control. Compared with using one of the control structures or algorithms alone, the active hybrid control (AHC) can achieve better vibration suppression performance. The following will introduce a piezoelectric active hybrid control design method, including an IFF control and a recursive least square (RLS) adaptive feedforward control, the feedback control realizes the sky-hook damping effect, and the adaptive feedforward control realizes the ground-based advance response.

#### 4.2 Piezoelectric IFF control in vibration suppression

Active feedback control can effectively solve the problem that the signal at the natural frequency is amplified, that is, the problem of formant attenuation. At present, the sky-hook technology is widely used in piezoelectric active feedback control. Generally, the sky-hook effect is established by absolute speed feedback control to reduce the formant peak value while maintaining high-frequency attenuation. This section introduces sky-hook technology based on piezoelectric actuators, which uses a combination of dynamic force sensors and piezoelectric actuators to design an integral force active control algorithm to achieve the control effect of sky-hook.

According to the structure above, the schematic diagram of the piezoelectric IFF control is shown in **Figure 8**. In **Figure 8**, the amount of elongation of the piezoelectric actuator is represented by  $\delta$ ,  $F$  represents the dynamic force signal. The active vibration control method of piezoelectric IFF control is: The dynamic force sensor collects the dynamic force signal, and after noise removal and filtering, the integral

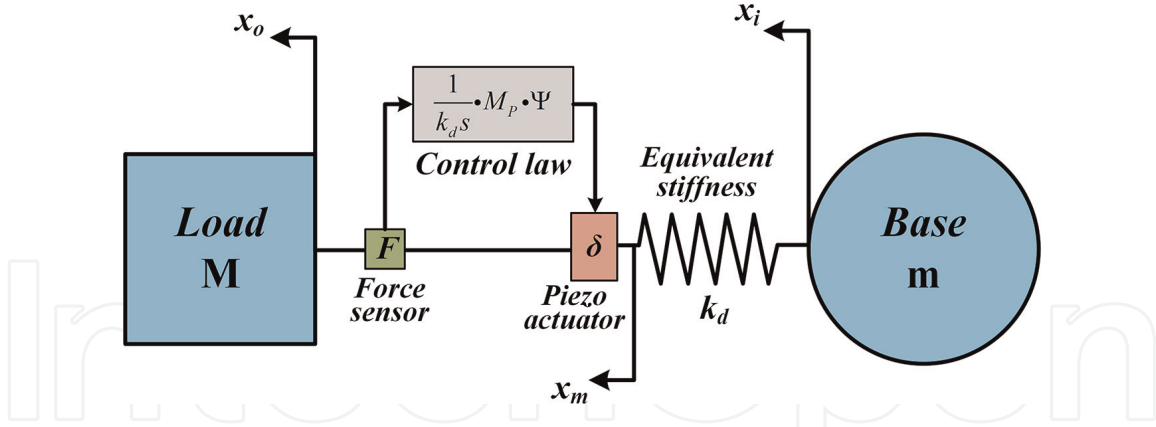


**Figure 8.**  
Schematic diagram of piezoelectric IFF principle.

calculation compensation is completed in the active control unit, and the control signal is output to the piezoelectric actuator to complete the piezoelectric active feedback control.

The IFF control law based on sky-hook damping technology is:

$$\sigma_{IFF} = \frac{1}{k_d s} \cdot \Psi \cdot F = \frac{1}{k_d s} \cdot M_p \cdot \Psi \cdot s^2 = \frac{1}{k_d s} \cdot k_i \cdot s^2 \quad (14)$$

where  $k_i = M_p \cdot \Psi$  is the integral gain coefficient of the IFF control.

According to **Figure 8**, the motion control equation of the piezoelectric IFF control system can be expressed as:

$$M s^2 x_o = -m s^2 x_i = k_d (x_i - x_m) = F \quad (15)$$

$$\delta = x_o - x_m \quad (16)$$

The open-loop transfer function between the elongation  $\delta$  of the piezoelectric actuator and the output  $F$  of the force sensor can be expressed as:

$$\frac{F}{\delta} = k_d \frac{M m s^2}{M m s^2 + k_d (M + m)} \quad (17)$$

According to the integral gain coefficient of the IFF algorithm in Eq. (14), after sorting and calculation, the displacement  $x_m$  of the middle section can be obtained as:

$$x_m = \frac{s x_o + k_i x_i}{s + k_i} = \frac{s x_o + M_p \cdot \Psi \cdot x_i}{s + M_p \cdot \Psi} \quad (18)$$

According to the above derivation, the transmissibility curve of the piezoelectric vibration isolation system under the IFF control algorithm is:

$$T_{C-IFF}(s) = \frac{c s + k_d}{M_p s^2 + (c + k_i) s + k_d} = \frac{1}{s^2 (1/\omega_n^2) + s (\Psi/\omega_n^2) + 1} \quad (19)$$

$$\omega_n = \sqrt{\frac{k_d}{M_p}} \quad (20)$$

where  $\omega_n$  is the natural frequency of the passive vibration isolation system. When the gain factor  $\Psi \gg c$ , the equivalent damping  $c$  of the system can be ignored.

The natural frequency and damping ratio of the piezoelectric vibration isolation system under the IFF control algorithm are expressed as:

$$\omega_p = \sqrt{\frac{k}{M_p}} = \omega_n \quad (21)$$

$$\zeta_p = \frac{c + k_i}{2\sqrt{km}} = \frac{M_p \cdot \Psi}{2\sqrt{km}} = \frac{\Psi}{2} \sqrt{\frac{M_p}{k}} = \frac{\Psi}{2\omega_n} \quad (22)$$

The natural frequency of the vibration isolation system under IFF control is consistent with the natural frequency of the passive system and does not change. The damping ratio of the vibration isolation system under the IFF control is proportional to the integral gain coefficient. By increasing the integral gain coefficient, the formant peak value at the natural frequency can be effectively reduced to achieve the sky-hook effect. It is worth noting that an excessively large gain coefficient will lead to system stability errors, making the vibration isolation system unstable.

According to the theoretical analysis of IFF, the simulation analysis is carried out in Matlab. The passive system parameters are shown in **Table 1**, and the parameters of the subsequent simulation are also consistent with **Table 1**. The simulation results are shown in **Figure 9**. It can be found that with the increase of the integral gain coefficient, the value of the resonance peak of the vibration isolation system decreases continuously, which plays a good role in suppressing vibration. This shows that the piezoelectric IFF control can achieve the effect of sky-hook damping control and can effectively suppress the formant.

#### 4.3 Piezoelectric RLS adaptive feedforward control in vibration suppression

The most direct way to improve the performance of feedback control is to increase its feedback gain. However, with the increase of the feedback gain, a large steady-state error will be introduced into the system. Therefore, a ground-based feedforward control strategy emerges as the times require. The ground-based feedforward control can effectively improve the local frequency-domain vibration suppression performance of the system by predicting the vibration signal in advance and implementing active control in the active algorithm. In piezoelectric feedforward control, the use of adaptive feedforward control is an extremely effective method. This section introduces an RLS adaptive feedforward control method.

The adaptive controller  $F_{ff} = F[y_i(k), d(k), y_o(k)]$  is a finite impulse response filter (FIR), also known as a transversal filter. For the observation signal that changes with time  $i$ , the tap weight vector  $w(n)$  of the transversal filter must be time-varying.

Simulation type	Passive Parameters
Load Mass (Kg)	1
System Stiffness (N/m)	3.41e4
System Damping (N.m/s)	7.65

**Table 1.**  
 Simulation parameters of single-degree-of-freedom passive vibration isolation system.

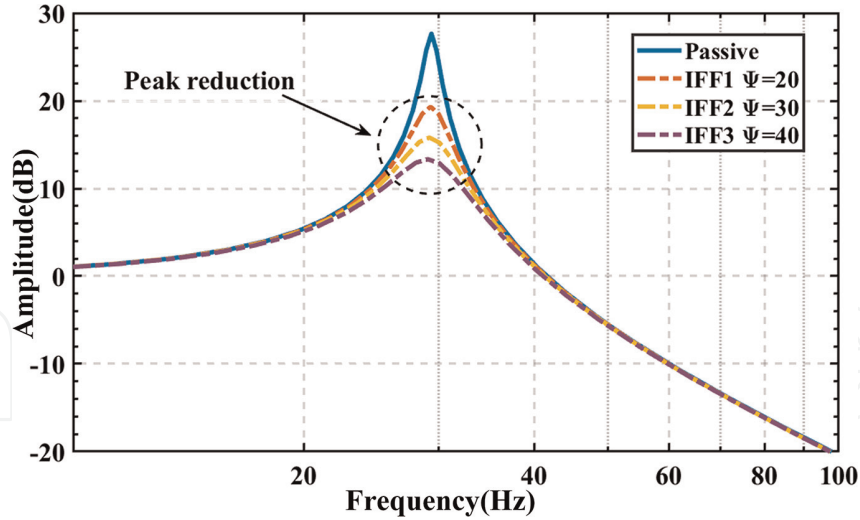


**Figure 9.**  
Transmittance curve of piezoelectric vibration isolation system under passive control and IFF control.

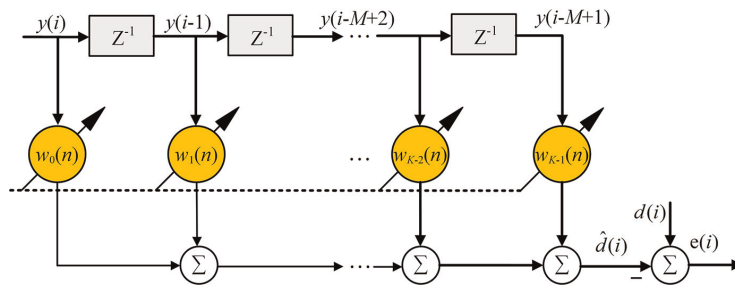


**Figure 10.**  
Transverse filter with time-varying tap weights.

To keep the adaptive controller in an optimal state, that is, to keep the gradient function of the cost function close to zero, the variable parameters must converge to the optimal value in real-time. Therefore, the filter used in the RLS algorithm is a transversal filter with time-varying tap weights. **Figure 10** shows the structure diagram of the transversal filter with time-varying tap weights.

The RLS adaptive control algorithm is a transversal filter based on the least-squares criterion. The algorithm recursively deduces the weight vector of the current time according to the filter tap weight vector of the previous time. Assuming that  $N$  data  $y(1), y(2), \dots, y(i), \dots, y(N)$  are known, the data is filtered with an  $M$ -order transversal filter with time-varying tap weights to get estimate the desired signals  $d(1), d(2), \dots, d(i), \dots, d(N)$ . Then the estimate of the expected response can be expressed as:

$$\hat{d}(i) = \sum_{j=0}^{M-1} w_j(n)y(i-j) = \mathbf{w}^T(n)\mathbf{y}(i) \quad (23)$$

where  $w_j(n)$  is the tap weight of the  $M$ -order transversal filter with time-varying tap weights,  $\mathbf{w}(n)$  is the tap weight vector of the filter with time-varying tap weights, and  $\mathbf{y}(i)$  is the tap input vector of the filter with time-varying tap weights at the  $i$ -th time, and are respectively:

$$\mathbf{w}(n) = [w_0(n), w_1(n), \dots, w_{M-1}(n)]^T \quad (24)$$



$$Y(i) = [y(i), y(i-1), \dots, y(i - M + 1)]^T \quad (25)$$

Then the estimated error of the filter with time-varying tap weights can be written as:

$$e(i) = d(i) - \hat{d}(i) = d(i) - \sum_{j=0}^{M-1} w_j(n)y(i-j) = d(i) - \mathbf{w}^T(n)\mathbf{y}(i) \quad (26)$$

Then the cost function under the least-squares criterion using the pre-windowing method can be expressed as:

$$\xi(n) = \sum_{i=1}^n \lambda^{n-i} e^2(i) \quad (27)$$

where  $\lambda$  is the forgetting factor, the value range is  $0 \leq \lambda \leq 1$ .

The RLS adaptive feedforward controller is built-in Matlab for simulation, and the simulation results are shown in **Figure 11**. Under the action of piezoelectric RLS adaptive feedforward control, the effective suppression rate of active control to amplitude can reach 80%, which is obviously better than passive control.

#### 4.4 Piezoelectric active hybrid controller

After the above description of IFF control and RLS adaptive feedforward control, a design scheme of piezoelectric AHC can be given. The block diagram of the AHC is shown in **Figure 12**. The principle is as follows: Given an additional external excitation signal, the signal  $y(n)$  is measured with a feedforward sensor. Design a transversal filter  $C(z^{-1})$  with time-varying tap weights, and continuously estimate the expected response  $d(i)$  by fitting the tap weight vector  $\mathbf{w}(n)$  constantly changing. By iteratively deriving the least squares estimated tap weight vector  $\mathbf{w}(n)$ , the square weighted sum of the estimated error  $e(i)$  (that is, the platform vibration error of the load platform) under this system is obtained to be the smallest, thereby, ensuring the platform vibration error of the load platform. The feedforward control loop finally generates

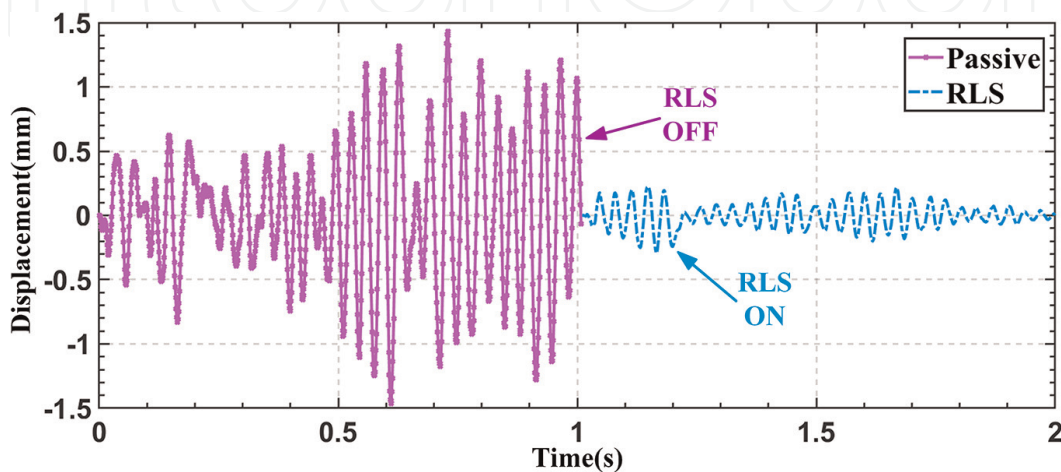


**Figure 11.**  
 Time domain comparison of RLS adaptive feedforward control and passive control.

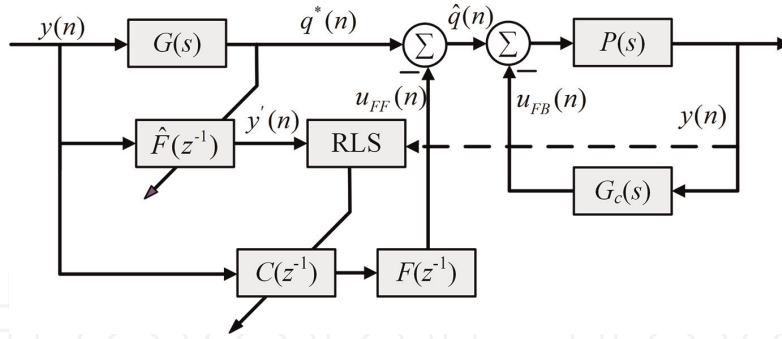


**Figure 12.**  
Piezoelectric AHC block diagram.

the feedforward control signal  $u_{FF}(n)$ , which is converted by the piezoelectric brake into an actual force acting on the system, which is opposite to the direct interference generated by the feedforward, thereby, eliminating the system vibration caused by the feedforward source. The feedback control loop performs compensation control on the error signal according to the feedback controller.

As shown in **Figure 12**,  $G(s)$  is the structural open-loop transfer function,  $P(s)$  is the structural closed-loop transfer function,  $G_c(s)$  is the feedback controller,  $C(z^{-1})$  is a transversal filter,  $F(z^{-1})$  is the transfer function from the feedforward control force to the vibration isolation system,  $\hat{F}(z^{-1})$  is the model of  $F(z^{-1})$  function with M-order identification,  $y(n)$  is an additional external stimulus,  $q^*(n)$  is the vibration response of the external excitation signal to the open-loop transfer function  $G(s)$  of the structure,  $u_{FF}(n)$  is the feedforward control output force,  $u_{FB}(n)$  is the feedback control output force,  $\hat{q}(n)$  is the first response error, and is the residual vibration error of the table after feedforward control,  $q(n)$  is the second error response, and is the residual vibration error of the table after entering the hybrid control.

According to Eq. (26), combined with the AHC block diagram, the system error  $e'(n)$  can be equivalent to the first residual vibration error response  $\hat{q}(n)$ , that is, the table residual vibration error after feedforward control:

$$e'(n) = \hat{q}(n) = q^*(n) - u_{FF}(n) = q^*(n) - \mathbf{w}^T(n)\mathbf{y}(n) \quad (28)$$

In the real-time control of the active vibration system, due to the real-time control operation of the system, the sensor can only measure the vibration signal of the ground foundation and the vibration signal after the active hybrid control of the table, and cannot directly measure the vibration response  $q^*(n)$  from the ground vibration signal to the open-loop transfer function  $G(s)$ . Therefore, the signal transfer can be estimated by the model reference function  $\hat{F}(z^{-1})$ :

$$q^*(n) \doteq y'(n) = y(n)\hat{F}(z^{-1}) \quad (29)$$

Then the system expansion error  $e(n)$  can be equivalent to the second error response  $q(n)$ , that is, the residual vibration error of the table after AHC:

$$e(n) = q(n) = e'(n) \frac{P(s)}{1 + P(s)G_c(s)} = \hat{q}(n) \frac{P(s)}{1 + P(s)G_c(s)} \quad (30)$$

According to Eq. (27), the cost function after using AHC is:

$$\xi(n) = \sum_{i=1}^n \lambda^{n-i} e^2(i) = \sum_{i=1}^n \lambda^{n-i} \left[ \frac{P(s)}{1 + P(s)G_c(s)} \right]^2 e^2(i) \quad (31)$$

The goal of the adaptive feedforward control algorithm is to find an optimal discrete filter and optimal weights so that the objective function of the cost function can be minimized, that is, the gradient of the cost function is zero:

$$\nabla_{\mathbf{w}_k} \xi = \frac{\partial \xi}{\partial \mathbf{w}_k} = -2 \left[ \frac{P(s)}{1 + P(s)G_c(s)} \right]^2 \sum_{i=1}^N \{ \lambda^{N-i} \mathbf{y}(i) [\mathbf{q}^*(i) - \mathbf{w}^T(i) \mathbf{y}(i)] \} = \mathbf{R}(n) \mathbf{w}(n) - \mathbf{r}(n) \quad (32)$$

$$\mathbf{R}(n) = \sum_{i=1}^n \lambda^{n-i} \mathbf{y}(i) \mathbf{y}^T(i) = \lambda \mathbf{R}(n-1) + \mathbf{y}(n) \mathbf{y}^T(n) \quad (33)$$

$$\mathbf{r}(n) = \sum_{i=1}^n \lambda^{n-i} \mathbf{y}(i) \mathbf{q}^*(i) = \lambda \mathbf{r}(n-1) + \mathbf{y}(n) \mathbf{q}^*(n) \quad (34)$$

where  $\mathbf{R}(n)$  is the autocorrelation matrix of the interference signal, and  $\mathbf{r}(n)$  is the cross-correlation matrix of the interference signal and the feedforward source signal.

Then, the gradient of Eq. (32) is zero, and the arrangement can be obtained:

$$\hat{\mathbf{w}}(n) = \mathbf{R}^{-1}(n) \mathbf{r}(n) \quad (35)$$

For the convenience of description, define an inverse matrix  $\mathbf{B}(n) = \mathbf{R}^{-1}(n)$ , and the following expression can be obtained:

$$\begin{aligned} \mathbf{B}(n) = \mathbf{R}^{-1}(n) &= \lambda^{-1} \left[ \mathbf{B}(n-1) - \frac{\mathbf{B}(n-1) \mathbf{y}(n) \mathbf{y}^T(n) \mathbf{B}(n-1)}{\lambda + \mathbf{y}^T(n) \mathbf{B}(n-1) \mathbf{y}(n)} \right] \\ &= \lambda^{-1} [\mathbf{B}(n-1) - \mathbf{k}(n) \mathbf{y}^T(n) \mathbf{B}(n-1)] \end{aligned} \quad (36)$$

where  $\mathbf{k}(n)$  is called the gain vector, and its expression is:

$$\mathbf{k}(n) = \frac{\mathbf{B}(n-1) \mathbf{y}(n)}{\lambda + \mathbf{y}^T(n) \mathbf{B}(n-1) \mathbf{y}(n)} \quad (37)$$

According to Eqs. (35)–(37), when the optimal solution of the tap weight vector has been obtained, the update formula of the weight vector can be further derived:

$$\hat{\mathbf{w}}(n) = \mathbf{R}^{-1}(n) \mathbf{r}(n) = \mathbf{B}(n) \mathbf{r}(n) = \hat{\mathbf{w}}(n-1) + \mathbf{k}(n) [\mathbf{q}^*(n) - \mathbf{y}^T(n) \hat{\mathbf{w}}(n-1)] \quad (38)$$

Then, the initialization of the AHC algorithm is set to  $\hat{\mathbf{w}}(0) = \mathbf{0}$ ,  $\mathbf{B}(0) = \delta^{-1}$  and  $\delta$  be very small positive numbers. The iterative formula of the AHC algorithm can be sorted out:

$$\begin{cases} \mathbf{k}(n) = \frac{\mathbf{B}(n-1) \mathbf{y}(n)}{\lambda + \mathbf{y}^T(n) \mathbf{B}(n-1) \mathbf{y}(n)} \\ \mathbf{B}(n) = \lambda^{-1} [\mathbf{B}(n-1) - \mathbf{k}(n) \mathbf{y}^T(n) \mathbf{B}(n-1)] \\ \hat{\mathbf{w}}(n) = \hat{\mathbf{w}}(n-1) + \mathbf{k}(n) [\mathbf{q}^*(n) - \mathbf{y}^T(n) \hat{\mathbf{w}}(n-1)] \end{cases} \quad (39)$$

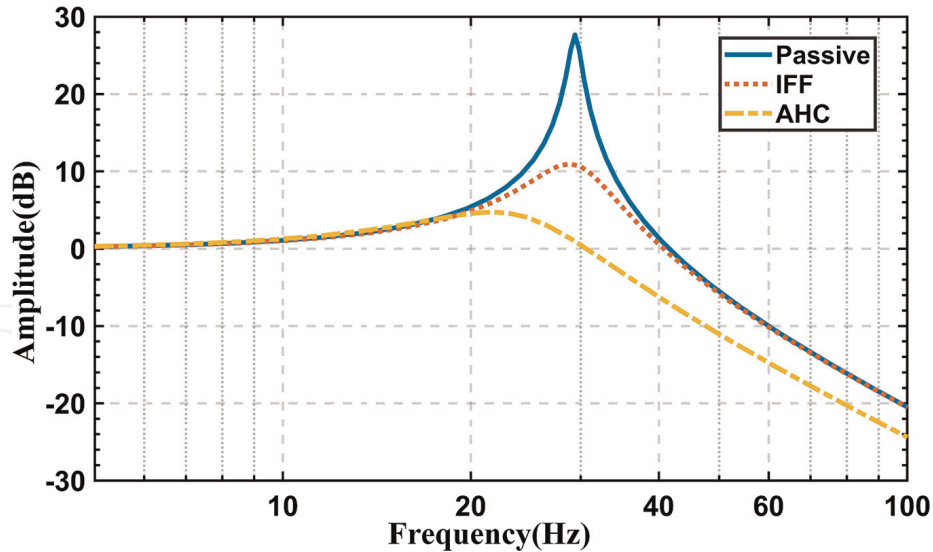


**Figure 13.**  
Simulation comparison curves of transmissibility under different control modes.

The simulation analysis of the AHC is carried out in Matlab, and the transmissibility curve in **Figure 13** can be obtained. In passive control, the vibration of the load platform is not effectively suppressed at all, and it is significantly attenuated at high frequencies. In the IFF control, the resonance peak at the natural frequency of the system is obviously suppressed, but the high-frequency attenuation is not improved. When the AHC is adopted, the formant of the system is further reduced, and the high frequency also shows a higher attenuation. The piezoelectric AHC has a better vibration isolation effect.

## 5. Experimental verification of piezoelectric active vibration suppression

### 5.1 Piezoelectric active vibration suppression system construction

Through the above theoretical analysis, to verify the vibration suppression performance of the proposed AHC algorithm in the piezoelectric vibration suppression system, an experimental test system is built, as shown in **Figure 14**. **Figure 14a** shows a single-degree-of-freedom piezoelectric vibration suppression platform, which mainly includes a piezoelectric actuator and a passive suppression unit. The piezoelectric actuator is responsible for active suppression, and the passive vibration isolation unit provides system stiffness. The two ends of the vibration suppression platform are respectively provided with a load mass block and a basic mass block, and the basic mass block relates to the output shaft of the vibration exciter so that the suppression platform can receive external excitation. The whole vibration suppression platform is suspended horizontally by hanging ropes, which can ensure the free boundary conditions and introduce the influence of low stiffness and damping.

**Figure 14b** shows a photograph of the experimental equipment setup integration. The experimental system is mainly divided into a real-time active control system and spectrum test and analysis system. The real-time active control system consists of a charge amplifier, an NI controller, and a piezoelectric driver. The active control process is as follows: The charge amplifier amplifies the feedback signal of the force sensor into



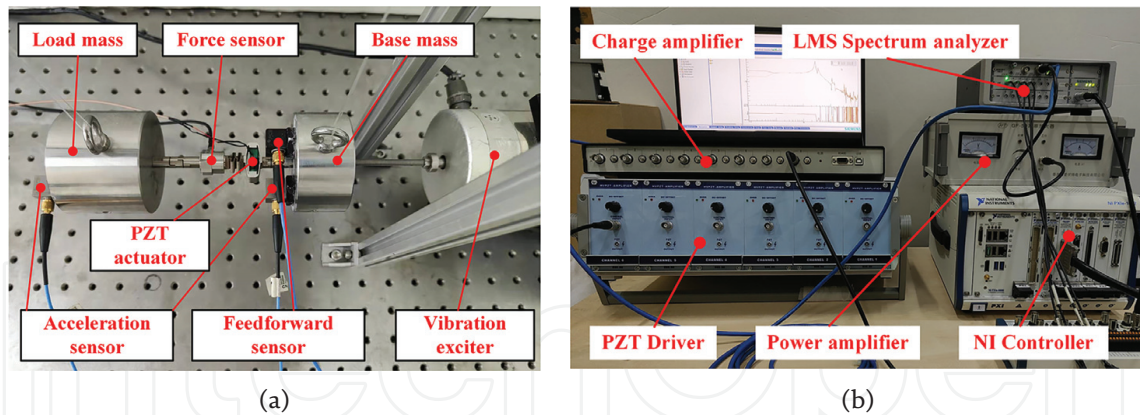


**Figure 14.**  
*Piezoelectric vibration suppression system: (a) single-degree-of-freedom piezoelectric vibration suppression platform; (b) experimental equipment.*

a voltage signal and outputs it to the NI controller. After the real-time active control algorithm in the NI controller, the control signal is generated and output to the piezoelectric driver for real-time active control of the linear piezoelectric actuator.

The spectrum test and analysis system include an LMS spectrum analyzer, an excitation signal output unit and an exciter power amplifier. The spectrum testing and analysis process are as follows: The LMS spectrum analyzer can output the excitation signal that simulates micro-vibration through the built-in simulation signal generator, and simulate the micro-vibration environment of the exciter through the exciter power amplifier. The LMS spectrum analyzer collects the vibration signals of the load platform and the base platform respectively through the acceleration sensor and performs postprocessing and spectrum analysis.

## 5.2 Verification of piezoelectric active vibration suppression performance

After completing the construction of the experimental system, the active control experiment was carried out in the piezoelectric suppression system. First, the system transmissibility curve is measured. The transmissibility curve measures the vibration transfer characteristics from the perspective of the frequency domain, which is a very important criterion. **Figure 15** shows the comparison curves of the system's transmissibility under different control methods. The blue line is the open-loop transmissibility curve of the system, which is not actively controlled and adopts pure passive vibration suppression. In the passive situation, the system has a peak near 30 Hz, which is the resonance peak, which means that the vibration amplitude will increase sharply here, and the vibration suppression effect is poor. At high frequencies, the passive transmissibility curve decays rapidly, which can be considered to have a suppressive effect. When IFF is used for piezoelectric active control, the resonance peak of the system at the natural frequency is attenuated to a certain extent, but the overall attenuation is not large, especially at high frequencies, the attenuation performance cannot be improved. When the AHC is used, the natural frequency of the system is moved forward, the resonance peak at the original natural frequency is greatly attenuated, and better attenuation is also reflected at high frequencies, which can effectively broaden the vibration isolation bandwidth. The specific values of the transmissibility curves under different control modes are shown in **Table 2**.



	Passive	IFF	AHC
Natural Frequency (Hz)	30	30	15
Resonance Peak (dB)	28	14.9	7.2
Decrease of Resonance Peak (dB)	/	13.1	20.8
Amplitude of 30 Hz (dB)	28	14.9	-1.9
Decrease of Amplitude in 30 Hz (dB)	/	13.1	29.9
Initial attenuation frequency (Hz)	43	43	22

**Table 2.**  
The specific value of the experimental transmissibility curve.

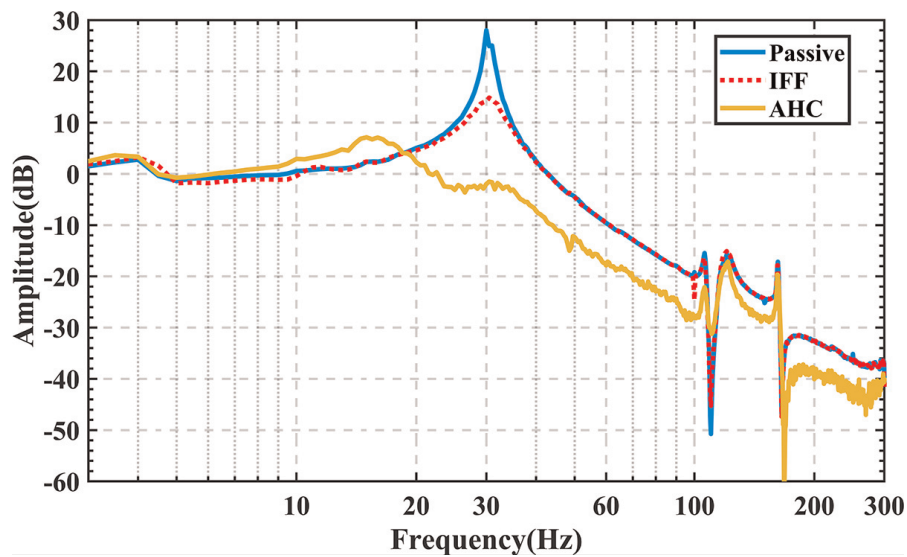


**Figure 15.**  
Transmissibility curves under passive, IFF, and AHC.

The time-domain vibration signal can reflect the control effect more intuitively, but more details in the frequency domain cannot be revealed. **Figure 16a** shows the time domain acceleration signal when the piezoelectric vibration suppression system is without active control. The red line is the basic excitation signal, the blue line is the load response signal, and the load response signal is the final control target. It can be found that the piezoelectric system can also achieve a certain vibration suppression effect through passive vibration suppression, but it is generally difficult to meet the application requirements. **Figure 16b** shows the time domain information of the piezoelectric vibration suppression system under the AHC. Compared with the pure passive vibration suppression, after the AHC is turned on, the vibration signal at the load end is greatly attenuated. In the piezoelectric vibration suppression system, the AHC method can greatly improve the vibration suppression performance.

**Figure 17** shows the self-power spectrum (PSD) curves with different control methods. In the case of passive vibration suppression (without control), the vibration energy of the load platform at the natural frequency is increased, which means that the vibration signal at the natural frequency is amplified. When AHC is used, the energy around the natural frequency is significantly suppressed because the piezoelectric actuator dissipates part of the energy.

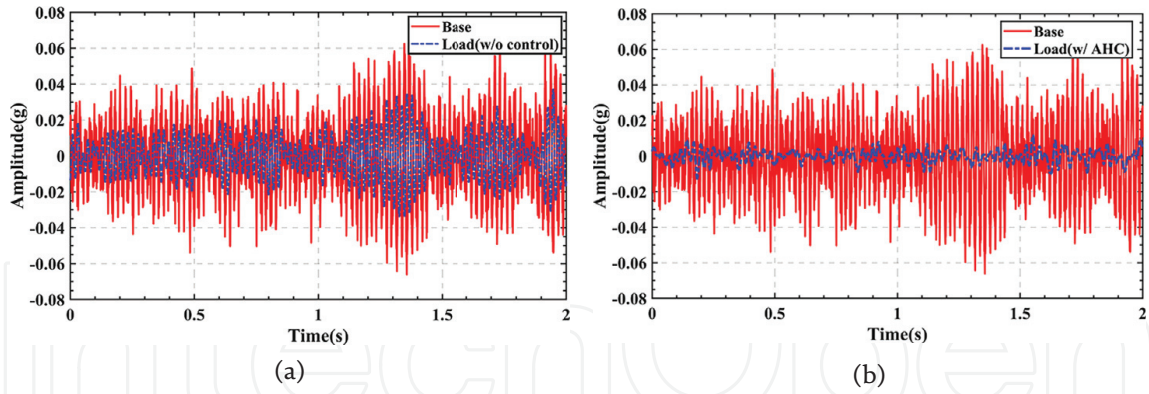


**Figure 16.**  
Time domain amplitude comparison curve: (a) without AHC; (b) with AHC.

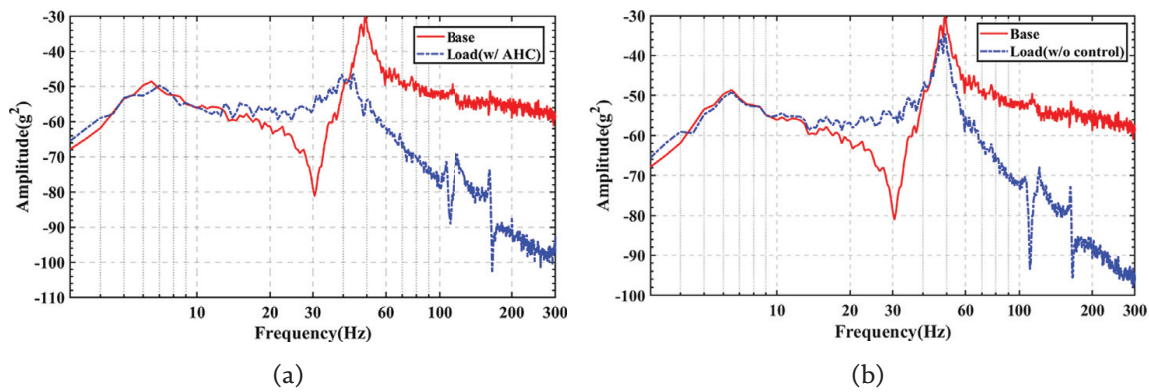


**Figure 17.**  
Self-power spectral density comparison curve: (a) without AHC; (b) with AHC.

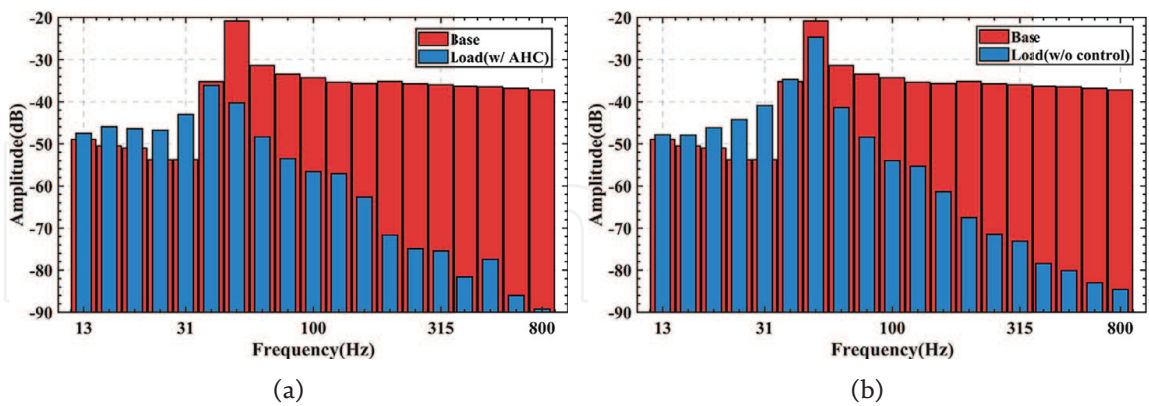


**Figure 18.**  
One-third octave comparison curve: (a) without AHC; (b) with AHC.

**Figure 18** shows one-third of octave curves with different control methods. When the piezoelectric vibration suppression system adopts passive vibration suppression (without control), the signal of the load platform near the natural frequency is significantly improved, which is also consistent with the self-power spectrum in **Figure 17**. When the AHC is turned on, the signal of the load platform near the natural frequency is attenuated, and the energy is dissipated by the piezoelectric actuator. This also shows that the piezoelectric AHC has a better inhibitory effect on the signal at the natural frequency.

## 6. Conclusions

In this chapter, the active vibration suppression of an active-passive composite vibration suppression system based on piezoelectric actuators is studied. On the basis of fully analyzing the characteristics of piezoelectric actuator and displacement amplifying mechanism and the dynamic model of vibration suppression system, an active composite control strategy based on IFF and RLS adaptive feedforward for vibration suppression on the piezoelectric system is discussed. The experimental results show that using the active control method, the vibration suppression system based on piezoelectric actuator has not only lower natural frequency, wider active vibration suppression bandwidth, but also reduces the value of the resonance peak, and maintains the attenuation rate at high frequency. Therefore, piezoelectric actuators are a good choice for vibration suppression, especially active vibration suppression.

## Acknowledgements

The work was supported by the National Natural Science Foundation of China [grant No. 61903242]; Shanghai Sailing Program [grant No. 19YF1416200].

## Conflict of interest

The author(s) declared no potential conflicts of interest with respect to the research, authorship, and/or publication of this article.

## Author details

Min Wang<sup>1,2\*</sup>, Songquan Liao<sup>1</sup>, Xuan Fang<sup>1</sup> and Shibo Fu<sup>1</sup>


1 School of Mechatronic Engineering and Automation, Shanghai University, Shanghai, China

2 Ministry of Education, Engineering Research Center of Unmanned Intelligent Marine Equipment, Shanghai, China

\*Address all correspondence to: xmwangmin@shu.edu.cn

## IntechOpen

---

© 2022 The Author(s). Licensee IntechOpen. This chapter is distributed under the terms of the Creative Commons Attribution License (<http://creativecommons.org/licenses/by/3.0>), which permits unrestricted use, distribution, and reproduction in any medium, provided the original work is properly cited. 

## References

- [1] Yan B, Brennan MJ, Elliott SJ, Ferguson NS. Active vibration isolation of a system with a distributed parameter isolator using absolute velocity feedback control. *Journal of Sound and Vibration*. 2010;**329**(10):1601-1614
- [2] Zuo L, Slotine JJE, Nayfeh SA. Model reaching adaptive control for vibration isolation. *IEEE Transactions on Control Systems Technology*. 2005;**13**(4):611-617
- [3] Burkan R, Ozguney OC, Ozbek C. Model reaching adaptive-robust control law for vibration isolation systems with parametric uncertainty. *Journal of Vibroengineering*. 2018;**20**(1):300-309
- [4] Sang H, Yang C, Liu F, Yun J, Jin G. A fuzzy neural network sliding mode controller for vibration suppression in robotically assisted minimally invasive surgery. *International Journal of Medical Robotics and Computer Assisted Surgery*. 2016;**12**(4):670-679
- [5] Yang L, Lou J, Zhu S. Researches on magnetostrictive hybrid vibration isolation system based on sliding mode algorithm. In: Wen Z, Li T, editors. *Foundations of Intelligent Systems* (iske 2013) [Internet]. Berlin: Springer-Verlag Berlin; 2014. pp. 1095-1106. Available from: <https://www.webofscience.com/wos/alldb/summary/1ba7f755-0d14-4def-ada3-274c2d75275f-201be7ef/relevance/1> [cited 2022 Jan 22]
- [6] Wei K, Meng G, Zhang W, Zhou S. Vibration characteristics of rotating sandwich beams filled with electrorheological fluids. *Journal of Intelligent Material Systems and Structures*. 2007;**18**(11):1165-1173
- [7] Manoharan R, Vasudevan R, Jeevanantham AK. Dynamic characterization of a laminated composite magnetorheological fluid sandwich plate. *Smart Materials and Structures*. 2014;**23**(2):025022
- [8] Damanpack AR, Bodaghi M, Aghdam MM, Shakeni M. On the vibration control capability of shape memory alloy composite beams. *Composite Structures*. 2014;**110**:325-334
- [9] Ebrahimi MR, Moeinfar A, Shakeri M. Nonlinear free vibration of hybrid composite moving beams embedded with shape memory alloy fibers. *International Journal of Structural Stability and Dynamics*. 2016;**16**(7):1550032
- [10] Xu XS, Sun FM, Wang GP. The control and optimization Design of the Fish-like Underwater Robot with the aid of the Giant Magnetostrictive material actuator. *Journal of Vibration and Control*. 2009;**15**(10):1443-1462
- [11] Pan Y, Zhao X. Design and analysis of a GMM actuator for active vibration isolation. In: 2015 IEEE International Conference on Mechatronics and Automation [Internet]. New York: IEEE; 2015. pp. 357-361. Available from: <https://www.webofscience.com/wos/alldb/summary/8e1c2d38-d225-4850-8215-81e5f0e84b48-2012e459/relevance/1> [cited 2022 Jan 22]
- [12] Manjunath TC, Bandyopadhyay B. Vibration control of Timoshenko smart structures using multirate output feedback based discrete sliding mode control for SISO systems. *Journal of Sound and Vibration*. 2009;**326**(1-2):50-74
- [13] Wang C, Xie X, Chen Y, Zhang Z. Investigation on active vibration isolation of a Stewart platform with piezoelectric actuators. *Journal of Sound and Vibration*. 2016;**383**:1-19



- [14] Jiang X, Zhu Y. Mechanical amplifier for Giant Magnetostrictive materials and piezoelectric materials [J]. *Hydromechatronics Engineering*. 2013
- [15] Chen J, Zhang C, Xu M, Zi Y, Zhang X. Rhombic micro-displacement amplifier for piezoelectric actuator and its linear and hybrid model. *Mechanical Systems and Signal Processing (MSSP)*. 2015;**50–51**:580-593
- [16] Choi K-B, Lee JJ, Kim GH, Lim HJ, Kwon SG. Amplification ratio analysis of a bridge-type mechanical amplification mechanism based on a fully compliant model. *Mechanism and Machine Theory*. 2018;**121**:355-372
- [17] Nguyen P-B, Choi S-B. A novel rate-independent hysteresis model of a piezostack actuator using the congruency property. *Smart Materials and Structures*. 2011;**20**(5):055003
- [18] Wang DH, Zhu W, Yang Q. Linearization of stack piezoelectric ceramic actuators based on Bouc-wen model. *Journal of Intelligent Material Systems and Structures*. 2011;**22**(5):401-413
- [19] Badel A, Le Breton R, Formosa F, Hanene S, Lottin J. Precise positioning and active vibration isolation using piezoelectric actuator with hysteresis compensation. *Journal of Intelligent Material Systems and Structures*. 2014;**25**(2):155-163
- [20] Minggang G, Zhi Q, Yanlong L. Sliding mode control with perturbation estimation and hysteresis compensator based on Bouc-wen model in tackling fast-varying sinusoidal position control of a piezoelectric actuator. *Journal of Systems Science & Complexity*. 2016;**29**(02):367-381
- [21] Cheng L, Liu W, Yang C, Huang T, Hou Z-G, Tan M. A neural-network-based controller for piezoelectric-actuated stick-slip devices. *IEEE Transactions on Industrial Electronics*. 2018;**65**(3):2598-2607
- [22] Nakamura Y, Nakayama M, Yasuda M, Fujita T. Development of active six-degrees-of-freedom micro-vibration control system using hybrid actuators comprising air actuators and giant magnetostrictive actuators. *Smart Materials and Structures*. 2006;**15**(4):1133-1142
- [23] Nguyen V-Q, Choi S-M, Choi S-B, Moon S-J. Sliding mode control of a vibrating system using a hybrid active mount. *Proceedings of the Institution of Mechanical Engineers Part C Journal of Engineering Mechanical Engineering Science*. 2009;**223**(6):1327-1337
- [24] Jang D-D, Jung H-J, Shin Y-H, Moon S-J, Moon Y-J, Oh J. Feasibility study on a hybrid mount system with air springs and piezo-stack actuators for microvibration control. *Journal of Intelligent Material Systems and Structures*. 2012;**23**(5):515-526
- [25] McInroy JE. Modeling and design of flexure jointed Stewart platforms for control purposes. *IEEE/ASME Transactions on Mechatronics*. 2002;**7**(1):95-99
- [26] Preumont A, Horodincea M, Romanescu I, de Marneffe B, Avraam M, Deraemaeker A, et al. A six-axis single-stage active vibration isolator based on Stewart platform. *Journal of Sound and Vibration*. 2007;**300**(3–5):644-661
- [27] Yang X, Wu H, Chen B, Kang S, Cheng S. Dynamic modeling and decoupled control of a flexible Stewart platform for vibration isolation. *Journal of Sound and Vibration*. 2019;**439**:398-412